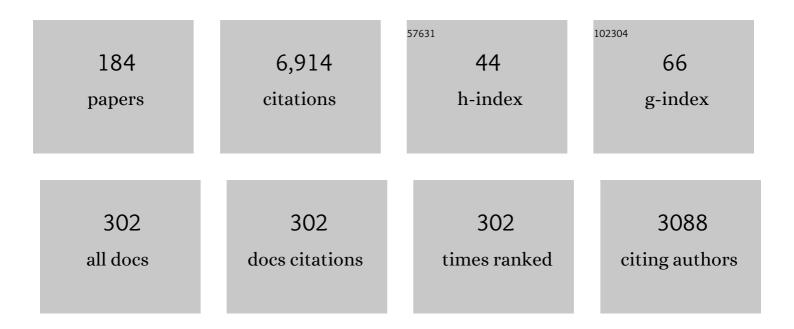
Martin Riese

List of Publications by Year in descending order

Source: https://exaly.com/author-pdf/669118/publications.pdf Version: 2024-02-01



#	Article	IF	CITATIONS
1	A case study on the impact of severe convective storms on the water vapor mixing ratio in the lower mid-latitude stratosphere observed in 2019 over Europe. Atmospheric Chemistry and Physics, 2022, 22, 1059-1079.	1.9	6
2	Stratospheric Moistening After 2000. Geophysical Research Letters, 2022, 49, .	1.5	13
3	Tropical Cyclones Reduce Ozone in the Tropopause Region Over the Western Pacific: An Analysis of 18AYears Ozonesonde Profiles. Earth's Future, 2021, 9, e2020EF001635.	2.4	9
4	Observation of cirrus clouds with GLORIA during the WISE campaign: detection methods and cirrus characterization. Atmospheric Measurement Techniques, 2021, 14, 3153-3168.	1.2	5
5	SOUTHTRAC-GW: An Airborne Field Campaign to Explore Gravity Wave Dynamics at the World's Strongest Hotspot. Bulletin of the American Meteorological Society, 2021, 102, E871-E893.	1.7	36
6	The stratospheric Brewer–Dobson circulation inferred from age of air in the ERA5 reanalysis. Atmospheric Chemistry and Physics, 2021, 21, 8393-8412.	1.9	24
7	Orographically induced spontaneous imbalance within the jet causing a large-scale gravity wave event. Atmospheric Chemistry and Physics, 2021, 21, 10393-10412.	1.9	9
8	3-D tomographic observations of Rossby wave breaking over the North Atlantic during the WISE aircraft campaign in 2017. Atmospheric Chemistry and Physics, 2021, 21, 10249-10272.	1.9	9
9	The semiannual oscillation (SAO) in the tropical middle atmosphere and its gravity wave driving in reanalyses and satellite observations. Atmospheric Chemistry and Physics, 2021, 21, 13763-13795.	1.9	22
10	Propagation paths and source distributions of resolved gravity waves in ECMWF-IFS analysis fields around the southern polar night jet. Atmospheric Chemistry and Physics, 2021, 21, 18641-18668.	1.9	15
11	AÂcomparison of OH nightglow volume emission rates as measured by SCIAMACHY and SABER. Atmospheric Measurement Techniques, 2020, 13, 3033-3042.	1.2	4
12	Dehydration and low ozone in the tropopause layer over the Asian monsoon caused by tropical cyclones: Lagrangian transport calculations using ERA-Interim and ERA5 reanalysis data. Atmospheric Chemistry and Physics, 2020, 20, 4133-4152.	1.9	35
13	Aerosol and cloud top height information of Envisat MIPAS measurements. Atmospheric Measurement Techniques, 2020, 13, 1243-1271.	1.2	6
14	FORUM: Unique Far-Infrared Satellite Observations to Better Understand How Earth Radiates Energy to Space. Bulletin of the American Meteorological Society, 2020, 101, E2030-E2046.	1.7	40
15	Thermally stable monolithic Doppler asymmetric spatial heterodyne interferometer: optical design and laboratory performance. Optics Express, 2020, 28, 19887.	1.7	8
16	Superposition of gravity waves with different propagation characteristics observed by airborne and space-borne infrared sounders. Atmospheric Chemistry and Physics, 2020, 20, 11469-11490.	1.9	11
17	A microphysics guide to cirrus – Part 2: Climatologies of clouds and humidity from observations. Atmospheric Chemistry and Physics, 2020, 20, 12569-12608.	1.9	80
18	Removing spurious inertial instability signals from gravity wave temperature perturbations using spectral filtering methods. Atmospheric Measurement Techniques, 2020, 13, 4927-4945.	1.2	15

#	Article	IF	CITATIONS
19	Cirrus cloud shape detection by tomographic extinction retrievals from infrared limb emission sounder measurements. Atmospheric Measurement Techniques, 2020, 13, 7025-7045.	1.2	3
20	Ammonium nitrate particles formed in upper troposphere from ground ammonia sources during Asian monsoons. Nature Geoscience, 2019, 12, 608-612.	5.4	95
21	Global analysis for periodic variations in gravity wave squared amplitudes and momentum fluxes in the middle atmosphere. Annales Geophysicae, 2019, 37, 487-506.	0.6	16
22	Tropospheric mixing and parametrization of unresolved convective updrafts as implemented in the Chemical Lagrangian Model of the Stratosphere (CLaMS v2.0). Geoscientific Model Development, 2019, 12, 2441-2462.	1.3	8
23	On the assembly and calibration of a spatial heterodyne interferometer for limb sounding of the middle atmosphere. CEAS Space Journal, 2019, 11, 525-531.	1.1	7
24	How robust are stratospheric age of air trends from different reanalyses?. Atmospheric Chemistry and Physics, 2019, 19, 6085-6105.	1.9	27
25	Sampling bias adjustment for sparsely sampled satellite measurements applied to ACE-FTS carbonyl sulfide observations. Atmospheric Measurement Techniques, 2019, 12, 2129-2138.	1.2	5
26	Multitimescale variations in modeled stratospheric water vapor derived from three modern reanalysis products. Atmospheric Chemistry and Physics, 2019, 19, 6509-6534.	1.9	23
27	Lagrangian simulations of the transport of young air masses to the top of the Asian monsoon anticyclone and into the tropical pipe. Atmospheric Chemistry and Physics, 2019, 19, 6007-6034.	1.9	57
28	Structural changes in the shallow and transition branch of the Brewer–Dobson circulation induced by El Niño. Atmospheric Chemistry and Physics, 2019, 19, 425-446.	1.9	27
29	Lagrangian simulation of ice particles and resulting dehydration in the polar winter stratosphere. Atmospheric Chemistry and Physics, 2019, 19, 543-563.	1.9	13
30	3-D tomographic limb sounder retrieval techniques: irregular grids and Laplacian regularisation. Atmospheric Measurement Techniques, 2019, 12, 853-872.	1.2	6
31	Evidence of small-scale quasi-isentropic mixing in ridges of extratropical baroclinic waves. Atmospheric Chemistry and Physics, 2019, 19, 12607-12630.	1.9	23
32	The efficiency of transport into the stratosphere via the Asian and North American summer monsoon circulations. Atmospheric Chemistry and Physics, 2019, 19, 15629-15649.	1.9	19
33	Global nighttime atomic oxygen abundances from GOMOS hydroxyl airglow measurements in the mesopause region. Atmospheric Chemistry and Physics, 2019, 19, 13891-13910.	1.9	5
34	AtmoCube A1: airglow measurements in the mesosphere and lower thermosphere by spatial heterodyne interferometry. Journal of Applied Remote Sensing, 2019, 13, 1.	0.6	5
35	Analysis and correction of distortions in a spatial heterodyne spectrometer system. Applied Optics, 2019, 58, 2190.	0.9	7
36	Optical design and performance analysis of a CubeSat-sized limb sounder utilizing a spatial heterodyne spectrometer for the measurement of mesospheric temperature. , 2019, , .		0

#	Article	IF	CITATIONS
37	Investigation on a SmallSat CMOS image sensor for atmospheric temperature measurement. , 2019, , .		6
38	Advances in the optical design of a spatial heterodyne interferometer deployed on a 6U-CubeSat for atmospheric research. , 2019, , .		0
39	Water vapor increase in the lower stratosphere of the Northern Hemisphere due to the Asian monsoon anticyclone observed during the TACTS/ESMVal campaigns. Atmospheric Chemistry and Physics, 2018, 18, 2973-2983.	1.9	22
40	Sensitivities of modelled water vapour in the lower stratosphere: temperature uncertainty, effects of horizontal transport and small-scale mixing. Atmospheric Chemistry and Physics, 2018, 18, 8505-8527.	1.9	17
41	A climatology of polar stratospheric cloud composition between 2002 and 2012 based on MIPAS/Envisat observations. Atmospheric Chemistry and Physics, 2018, 18, 5089-5113.	1.9	38
42	Limited angle tomography of mesoscale gravity waves by the infrared limb-sounder GLORIA. Atmospheric Measurement Techniques, 2018, 11, 4327-4344.	1.2	13
43	lce particle sampling from aircraft – influence of the probing position on the ice water content. Atmospheric Measurement Techniques, 2018, 11, 4015-4031.	1.2	21
44	Three-dimensional tomographic reconstruction of atmospheric gravity waves in the mesosphere and lower thermosphere (MLT). Atmospheric Measurement Techniques, 2018, 11, 3161-3175.	1.2	6
45	High tropospheric ozone in Lhasa within the Asian summer monsoon anticyclone in 2013: influence of convective transport and stratospheric intrusions. Atmospheric Chemistry and Physics, 2018, 18, 17979-17994.	1.9	30
46	A highly miniaturized satellite payload based on a spatial heterodyne spectrometer for atmospheric temperature measurements in the mesosphere and lower thermosphere. Atmospheric Measurement Techniques, 2018, 11, 3861-3870.	1.2	33
47	Response of stratospheric water vapor and ozone to the unusual timing of El Niño and the QBO disruption in 2015–2016. Atmospheric Chemistry and Physics, 2018, 18, 13055-13073.	1.9	48
48	Satellite observations of middle atmosphere–thermosphere vertical coupling by gravity waves. Annales Geophysicae, 2018, 36, 425-444.	0.6	45
49	El Niño Southern Oscillation influence on the Asian summer monsoon anticyclone. Atmospheric Chemistry and Physics, 2018, 18, 8079-8096.	1.9	15
50	GRACILE: a comprehensive climatology of atmospheric gravity wave parameters based on satellite limb soundings. Earth System Science Data, 2018, 10, 857-892.	3.7	91
51	A novel CubeSat payload for airglow measurements in the mesosphere and lower thermosphere. , 2018, , .		2
52	Effective wind and temperature retrieval from Doppler asymmetric spatial heterodyne spectrometer interferograms. Applied Optics, 2018, 57, 8829.	0.9	7
53	Upper tropospheric water vapour and its interaction with cirrus clouds as seen from IAGOS long-term routine in situ observations. Faraday Discussions, 2017, 200, 229-249.	1.6	16
54	Quantifying pollution transport from the Asian monsoon anticyclone into the lower stratosphere. Atmospheric Chemistry and Physics, 2017, 17, 7055-7066.	1.9	61

#	Article	IF	CITATIONS
55	Regionally Resolved Diagnostic of Transport: A Simplified Forward Model for CO2. Journals of the Atmospheric Sciences, 2017, 74, 2689-2700.	0.6	5
56	Shift of subtropical transport barriers explains observed hemispheric asymmetry of decadal trends of age of air. Atmospheric Chemistry and Physics, 2017, 17, 11177-11192.	1.9	34
57	Significant Contributions of Volcanic Aerosols to Decadal Changes in the Stratospheric Circulation. Geophysical Research Letters, 2017, 44, 10,780.	1.5	28
58	First tomographic observations of gravity waves by the infrared limb imager GLORIA. Atmospheric Chemistry and Physics, 2017, 17, 14937-14953.	1.9	51
59	Tomographic reconstruction of atmospheric gravity wave parameters from airglow observations. Atmospheric Measurement Techniques, 2017, 10, 4601-4612.	1.2	18
60	Infrared limb emission measurements of aerosol in the troposphere and stratosphere. Atmospheric Measurement Techniques, 2016, 9, 4399-4423.	1.2	24
61	Zonally resolved impact of ENSO on the stratospheric circulation and water vapor entry values. Journal of Geophysical Research D: Atmospheres, 2016, 121, 11,486.	1.2	27
62	Comparison of simulated and observed convective gravity waves. Journal of Geophysical Research D: Atmospheres, 2016, 121, 13,474.	1.2	15
63	The need for accurate longâ€ŧerm measurements of water vapor in the upper troposphere and lower stratosphere with global coverage. Earth's Future, 2016, 4, 25-32.	2.4	32
64	Long-range transport pathways of tropospheric source gases originating in Asia into the northern lower stratosphere during the Asian monsoon season 2012. Atmospheric Chemistry and Physics, 2016, 16, 15301-15325.	1.9	57
65	Impact of the Asian monsoon on the extratropical lower stratosphere: trace gas observations during TACTS over Europe 2012. Atmospheric Chemistry and Physics, 2016, 16, 10573-10589.	1.9	34
66	Tuning of a convective gravity wave source scheme based on HIRDLS observations. Atmospheric Chemistry and Physics, 2016, 16, 7335-7356.	1.9	33
67	Observations of PAN and its confinement in the Asian summer monsoon anticyclone in high spatial resolution. Atmospheric Chemistry and Physics, 2016, 16, 8389-8403.	1.9	36
68	Satellite observations of middle atmosphere gravity wave absolute momentum flux and of its vertical gradient during recent stratospheric warmings. Atmospheric Chemistry and Physics, 2016, 16, 9983-10019.	1.9	59
69	A multi-wavelength classification method for polar stratospheric cloud types using infrared limb spectra. Atmospheric Measurement Techniques, 2016, 9, 3619-3639.	1.2	21
70	Towards high resolution infrared limb sounding of the upper troposphere / lower stratosphere (UTLS). , 2016, , .		0
71	Nighttime atomic oxygen in the mesopause region retrieved from SCIAMACHY O(¹ S) green line measurements and its response to solar cycle variation. Journal of Geophysical Research: Space Physics, 2015, 120, 9057-9073.	0.8	17
72	Impact of stratospheric major warmings and the quasiâ€biennial oscillation on the variability of stratospheric water vapor. Geophysical Research Letters, 2015, 42, 4599-4607.	1.5	25

#	Article	IF	CITATIONS
73	Impact of different Asian source regions on the composition of the Asian monsoon anticyclone and of the extratropical lowermost stratosphere. Atmospheric Chemistry and Physics, 2015, 15, 13699-13716.	1.9	75
74	Impact of the 2009 major sudden stratospheric warming on the composition of the stratosphere. Atmospheric Chemistry and Physics, 2015, 15, 8695-8715.	1.9	32
75	Satellite observations of cirrus clouds in the Northern Hemisphere lowermost stratosphere. Atmospheric Chemistry and Physics, 2015, 15, 927-950.	1.9	37
76	A potential vorticity-based determination of the transport barrier in the Asian summer monsoon anticyclone. Atmospheric Chemistry and Physics, 2015, 15, 13145-13159.	1.9	78
77	New calibration noise suppression techniques for the GLORIA limb imager. Atmospheric Measurement Techniques, 2015, 8, 3147-3161.	1.2	4
78	Level 2 processing for the imaging Fourier transform spectrometer GLORIA: derivation and validation of temperature and trace gas volume mixing ratios from calibrated dynamics mode spectra. Atmospheric Measurement Techniques, 2015, 8, 2473-2489.	1.2	30
79	Validation of first chemistry mode retrieval results from the new limb-imaging FTS GLORIA with correlative MIPAS-STR observations. Atmospheric Measurement Techniques, 2015, 8, 2509-2520.	1.2	11
80	Hemispheric asymmetries and seasonality of mean age of air in the lower stratosphere: Deep versus shallow branch of the Brewerâ€Dobson circulation. Journal of Geophysical Research D: Atmospheres, 2015, 120, 2053-2066.	1.2	34
81	Quantifying the effects of mixing and residual circulation on trends of stratospheric mean age of air. Geophysical Research Letters, 2015, 42, 2047-2054.	1.5	69
82	Driving of the SAO by gravity waves as observed from satellite. Annales Geophysicae, 2015, 33, 483-504.	0.6	43
83	Retrieval of three-dimensional small-scale structures in upper-tropospheric/lower-stratospheric composition as measured by GLORIA. Atmospheric Measurement Techniques, 2015, 8, 81-95.	1.2	38
84	A comprehensive observational filter for satellite infrared limb sounding of gravity waves. Atmospheric Measurement Techniques, 2015, 8, 1491-1517.	1.2	36
85	Variability of stratospheric mean age of air and of the local effects of residual circulation and eddy mixing. Journal of Geophysical Research D: Atmospheres, 2015, 120, 716-733.	1.2	48
86	Tropical troposphere to stratosphere transport of carbon monoxide and long-lived trace species in the Chemical Lagrangian Model of the Stratosphere (CLaMS). Geoscientific Model Development, 2014, 7, 2895-2916.	1.3	104
87	Sea surface temperature as a proxy for convective gravity wave excitation: a study based on global gravity wave observations in the middle atmosphere. Annales Geophysicae, 2014, 32, 1373-1394.	0.6	14
88	Volcanic ash detection with infrared limb sounding: MIPAS observations and radiative transfer simulations. Atmospheric Measurement Techniques, 2014, 7, 1487-1507.	1.2	30
89	Gimballed Limb Observer for Radiance Imaging of the Atmosphere (GLORIA) scientific objectives. Atmospheric Measurement Techniques, 2014, 7, 1915-1928.	1.2	85
90	Instrument concept of the imaging Fourier transform spectrometer GLORIA. Atmospheric Measurement Techniques, 2014, 7, 3565-3577.	1.2	82

#	Article	IF	CITATIONS
91	Global distribution of atomic oxygen in the mesopause region as derived from SCIAMACHY O(¹ S) green line measurements. Geophysical Research Letters, 2014, 41, 6274-6280.	1.5	36
92	Fast transport from Southeast Asia boundary layer sources to northern Europe: rapid uplift in typhoons and eastward eddy shedding of the Asian monsoon anticyclone. Atmospheric Chemistry and Physics, 2014, 14, 12745-12762.	1.9	97
93	Differences in gravity wave drag between realistic oblique and assumed vertical propagation. Journal of Geophysical Research D: Atmospheres, 2014, 119, 10,081.	1.2	51
94	Interaction of gravity waves with the QBO: A satellite perspective. Journal of Geophysical Research D: Atmospheres, 2014, 119, 2329-2355.	1.2	109
95	Characteristics of gravity waves resolved by ECMWF. Atmospheric Chemistry and Physics, 2014, 14, 10483-10508.	1.9	78
96	Physical and Chemical Processes in the Upper Troposphere and Lower Stratosphere. The Reacting Atmosphere, 2014, , 19-25.	0.8	0
97	Scattering in infrared radiative transfer: A comparison between the spectrally averaging model JURASSIC and the line-by-line model KOPRA. Journal of Quantitative Spectroscopy and Radiative Transfer, 2013, 127, 102-118.	1.1	23
98	Role of gravity waves in the forcing of quasi twoâ€day waves in the mesosphere: An observational study. Journal of Geophysical Research D: Atmospheres, 2013, 118, 3467-3485.	1.2	76
99	Stratospheric loss and atmospheric lifetimes of CFC-11 and CFC-12 derived from satellite observations. Atmospheric Chemistry and Physics, 2013, 13, 4253-4263.	1.9	19
100	Assessment of the interannual variability and influence of the QBO and upwelling on tracer–tracer distributions of N ₂ O and O ₃ in the tropical lower stratosphere. Atmospheric Chemistry and Physics, 2013, 13, 3619-3641.	1.9	9
101	Filamentary structure in chemical tracer distributions near the subtropical jet following a wave breaking event. Atmospheric Chemistry and Physics, 2013, 13, 10517-10534.	1.9	30
102	Observations of filamentary structures near the vortex edge in the Arctic winter lower stratosphere. Atmospheric Chemistry and Physics, 2013, 13, 10859-10871.	1.9	12
103	Reconciliation of essential process parameters for an enhanced predictability of Arctic stratospheric ozone loss and its climate interactions (RECONCILE): activities and results. Atmospheric Chemistry and Physics, 2013, 13, 9233-9268.	1.9	88
104	Horizontal water vapor transport in the lower stratosphere from subtropics to high latitudes during boreal summer. Journal of Geophysical Research D: Atmospheres, 2013, 118, 8111-8127.	1.2	100
105	Extending water vapor trend observations over Boulder into the tropopause region: Trend uncertainties and resulting radiative forcing. Journal of Geophysical Research D: Atmospheres, 2013, 118, 11269-11284.	1.2	28
106	The Response of Atomic Hydrogen to Solar Radiation Changes. Springer Atmospheric Sciences, 2013, , 171-188.	0.4	6
107	CRISTA-NF measurements with unprecedented vertical resolution during the RECONCILE aircraft campaign. Atmospheric Measurement Techniques, 2012, 5, 1173-1191.	1.2	32
108	Backtrajectory reconstruction of water vapour and ozone in-situ observations in the TTL. Meteorologische Zeitschrift, 2012, 21, 239-244.	0.5	8

#	Article	IF	CITATIONS
109	Fast cloud parameter retrievals of MIPAS/Envisat. Atmospheric Chemistry and Physics, 2012, 12, 7135-7164.	1.9	37
110	Lidar observation and model simulation of a volcanic-ash-induced cirrus cloud during the Eyjafjallajökull eruption. Atmospheric Chemistry and Physics, 2012, 12, 10281-10294.	1.9	29
111	Tropospheric ozone trend over Beijing from 2002–2010: ozonesonde measurements and modeling analysis. Atmospheric Chemistry and Physics, 2012, 12, 8389-8399.	1.9	111
112	A stratospheric intrusion at the subtropical jet over the Mediterranean Sea: air-borne remote sensing observations and model results. Atmospheric Chemistry and Physics, 2012, 12, 8423-8438.	1.9	24
113	Impact of a possible future global hydrogen economy on Arctic stratospheric ozone loss. Energy and Environmental Science, 2012, 5, 6445.	15.6	28
114	Horizontal transport affecting trace gas seasonality in the Tropical Tropopause Layer (TTL). Journal of Geophysical Research, 2012, 117, .	3.3	80
115	Impact of uncertainties in atmospheric mixing on simulated UTLS composition and related radiative effects. Journal of Geophysical Research, 2012, 117, .	3.3	260
116	Implications for atmospheric dynamics derived from global observations of gravity wave momentum flux in stratosphere and mesosphere. Journal of Geophysical Research, 2011, 116, .	3.3	203
117	Insight from ozone and water vapour on transport in the tropical tropopause layer (TTL). Atmospheric Chemistry and Physics, 2011, 11, 407-419.	1.9	71
118	A 3-D tomographic retrieval approach with advection compensation for the air-borne limb-imager GLORIA. Atmospheric Measurement Techniques, 2011, 4, 2509-2529.	1.2	61
119	Towards a 3-D tomographic retrieval for the air-borne limb-imager GLORIA. Atmospheric Measurement Techniques, 2010, 3, 1647-1665.	1.2	90
120	CRISTA-NF measurements during the AMMA-SCOUT-O3 aircraft campaign. Atmospheric Measurement Techniques, 2010, 3, 1437-1455.	1.2	22
121	What causes the irregular cycle of the atmospheric tape recorder signal in HCN?. Geophysical Research Letters, 2010, 37, .	1.5	22
122	Tomographic retrieval approach for mesoscale gravity wave observations by the PREMIER Infrared Limb-Sounder. Atmospheric Measurement Techniques, 2010, 3, 339-354.	1.2	33
123	New perspectives on gravity wave remote sensing by spaceborne infrared limb imaging. Atmospheric Measurement Techniques, 2009, 2, 299-311.	1.2	63
124	CRISTA-NF measurements of water vapor during the SCOUT-O3 Tropical Aircraft Campaign. Advances in Space Research, 2009, 43, 74-81.	1.2	28
125	Radiance calibration of CRISTA-NF. Advances in Space Research, 2009, 43, 1910-1917.	1.2	11
126	Global ray tracing simulations of the SABER gravity wave climatology. Journal of Geophysical Research, 2009, 114, .	3.3	120

#	Article	IF	CITATIONS
127	Gravity waves resolved in ECMWF and measured by SABER. Geophysical Research Letters, 2009, 36, .	1.5	52
128	Spectral wave analysis at the mesopause from SCIAMACHY airglow data compared to SABER temperature spectra. Annales Geophysicae, 2009, 27, 407-416.	0.6	30
129	Chemical heating rates derived from SCIAMACHY vibrationally excited OH limb emission spectra. Advances in Space Research, 2008, 41, 1914-1920.	1.2	20
130	High resolution limb observations of clouds by the CRISTA-NF experiment during the SCOUT-O3 tropical aircraft campaign. Advances in Space Research, 2008, 42, 1765-1775.	1.2	32
131	Sensitivity of Arctic ozone loss to stratospheric H ₂ 0. Geophysical Research Letters, 2008, 35, .	1.5	28
132	Model simulations of stratospheric ozone loss caused by enhanced mesospheric NO _x during Arctic Winter 2003/2004. Atmospheric Chemistry and Physics, 2008, 8, 5279-5293.	1.9	33
133	Envisat MIPAS measurements of CFC-11: retrieval, validation, and climatology. Atmospheric Chemistry and Physics, 2008, 8, 3671-3688.	1.9	77
134	Contribution of mixing to upward transport across the tropical tropopause layer (TTL). Atmospheric Chemistry and Physics, 2007, 7, 3285-3308.	1.9	109
135	Ozone loss driven by nitrogen oxides and triggered by stratospheric warmings can outweigh the effect of halogens. Journal of Geophysical Research, 2007, 112, .	3.3	38
136	Long-term changes of methane and hydrogen in the stratosphere in the period 1978–2003 and their impact on the abundance of stratospheric water vapor. Journal of Geophysical Research, 2006, 111, .	3.3	59
137	Chemical ozone loss in a chemistry-climate model from 1960 to 1999. Geophysical Research Letters, 2006, 33, .	1.5	17
138	Seasonal cycles and variability of O ₃ and H ₂ O in the UT/LMS during SPURT. Atmospheric Chemistry and Physics, 2006, 6, 109-125.	1.9	48
139	Instrument concept and preliminary performance analysis of GLORIA. Advances in Space Research, 2006, 37, 2287-2291.	1.2	47
140	Vibrationally excited ozone in the middle atmosphere. Journal of Atmospheric and Solar-Terrestrial Physics, 2006, 68, 202-212.	0.6	26
141	Tropopause to mesopause gravity waves in August: Measurement and modeling. Journal of Atmospheric and Solar-Terrestrial Physics, 2006, 68, 1730-1751.	0.6	77
142	Long-term changes of hydrogen-containing species in the stratosphere. Journal of Atmospheric and Solar-Terrestrial Physics, 2006, 68, 1973-1979.	0.6	11
143	Intercomparison between Lagrangian and Eulerian simulations of the development of mid-latitude streamers as observed by CRISTA. Atmospheric Chemistry and Physics, 2005, 5, 85-95.	1.9	19
144	Retrieval of CFC-11 and CFC-12 from Envisat MIPAS observations by means of rapid radiative transfer calculations. Advances in Space Research, 2005, 36, 915-921.	1.2	24

#	Article	IF	CITATIONS
145	MIPAS observation of polar stratospheric clouds in the Arctic 2002/2003 and Antarctic 2003 winters. Advances in Space Research, 2005, 36, 868-878.	1.2	21
146	GLObal limb Radiance Imager for the Atmosphere (GLORIA): Scientific objectives. Advances in Space Research, 2005, 36, 989-995.	1.2	68
147	How homogeneous and isotropic is stratospheric mixing? Comparison of CRISTA-1 observations with transport studies based on the Chemical Lagrangian Model of the Stratosphere (CLaMS). Quarterly Journal of the Royal Meteorological Society, 2005, 131, 565-579.	1.0	20
148	A case study of trace gas transports near the tropopause. Advances in Space Research, 2004, 33, 1053-1057.	1.2	3
149	Quantitative transport studies based on trace gas assimilation. Advances in Space Research, 2004, 33, 1068-1072.	1.2	7
150	Cryogenic infrared spectrometers and telescopes for the atmosphere: new frontiers. , 2004, , .		23
151	Retrieval of chlorofluorocarbon distributions from Envisat MIPAS measurements. , 2004, , .		3
152	Retrieval of Upper Tropospheric H2O from CRISTA-2 Observations. , 2004, , 149-153.		0
153	Stratospheric transport by planetary wave mixing as observed during CRISTA-2. Journal of Geophysical Research, 2002, 107, CRI 7-1-CRI 7-13.	3.3	39
154	The CRISTA-2 mission. Journal of Geophysical Research, 2002, 107, CRI 1-1-CRI 1-12.	3.3	84
155	CRISTA observations of cirrus clouds around the tropopause. Journal of Geophysical Research, 2002, 107, CRI 2-1-CRI 2-18.	3.3	51
156	Space-based measurements of stratospheric mountain waves by CRISTA 1. Sensitivity, analysis method, and a case study. Journal of Geophysical Research, 2002, 107, CRI 6-1-CRI 6-23.	3.3	227
157	Water vapor at the tropopause during the CRISTA 2 mission. Journal of Geophysical Research, 2002, 107, CRI 4-1-CRI 4-18.	3.3	26
158	NOypartitioning and aerosol influences in the stratosphere. Journal of Geophysical Research, 2002, 107, CRI 11-1-CRI 11-14.	3.3	10
159	CRISTA-2 observations of the South Polar Vortex in winter 1997: A new dataset for polar process studies. Geophysical Research Letters, 2001, 28, 3159-3162.	1.5	42
160	Comparison of satellite ozone observations in coincident air masses in early November 1994. Journal of Geophysical Research, 2001, 106, 9923-9943.	3.3	40
161	<title>Trace gas densities and dynamics at and above the tropopause as derived from CRISTA data</title> .,2001,,.		3
162	Tracer structures in the southern hemispheric middle stratosphere observed by CRISTA-1. Advances in Space Research, 2001, 27, 1623-1628.	1.2	2

#	Article	IF	CITATIONS
163	A detection method for cirrus clouds using CRISTA 1 and 2 measurements. Advances in Space Research, 2001, 27, 1629-1634.	1.2	10
164	Retrieval of water vapor in the tropopause region from CRISTA measurements. Advances in Space Research, 2001, 27, 1635-1640.	1.2	11
165	Three-dimensional model simulations of CRISTA trace gas measurements. Advances in Space Research, 2000, 26, 971-974.	1.2	2
166	Planetary wave two signatures in CRISTA 2 ozone and temperature data. Geophysical Monograph Series, 2000, , 319-325.	0.1	14
167	Modeling the diurnal tide for the Cryogenic Infrared Spectrometers and Telescopes for the Atmosphere (CRISTA) 1 time period. Journal of Geophysical Research, 2000, 105, 24917-24929.	3.3	34
168	Evidence of H2O nonlocal thermodynamic equilibrium emission near 6.4 μm as measured by cryogenic infrared spectrometers and telescopes for the atmosphere (CRISTA 1). Journal of Geophysical Research, 2000, 105, 29003-29021.	3.3	8
169	Modeling of nitrogen species measured by CRISTA. Geophysical Research Letters, 2000, 27, 2221-2224.	1.5	7
170	Hemispheric asymmetry of chemical species and its effect on stratospheric ozone: Emphasis on halogen loading. Advances in Space Research, 1999, 24, 1631-1636.	1.2	2
171	Cryogenic Infrared Spectrometers and Telescopes for the Atmosphere (CRISTA) experiment and middle atmosphere variability. Journal of Geophysical Research, 1999, 104, 16311-16325.	3.3	177
172	Cryogenic Infrared Spectrometers and Telescopes for the Atmosphere (CRISTA) data processing and atmospheric temperature and trace gas retrieval. Journal of Geophysical Research, 1999, 104, 16349-16367.	3.3	130
173	Tidal signatures in temperature data from CRISTA 1 mission. Journal of Geophysical Research, 1999, 104, 16391-16403.	3.3	51
174	Intercomparison of satellite and aircraft observations of ozone, CFC-11, and NOyusing trajectory mapping. Journal of Geophysical Research, 1999, 104, 16379-16390.	3.3	24
175	Three-dimensional simulation of stratospheric trace gas distributions measured by CRISTA. Journal of Geophysical Research, 1999, 104, 16419-16435.	3.3	38
176	Cryogenic Infrared Spectrometers and Telescopes for the Atmosphere (CRISTA) observations of tracer transport by inertially unstable circulations. Journal of Geophysical Research, 1999, 104, 19171-19182.	3.3	20
177	Implications of Satellite OH Observations for Middle Atmospheric H2O and Ozone. Science, 1997, 277, 1967-1970.	6.0	114
178	CRISTA ozone measurements/validation. Advances in Space Research, 1997, 19, 567-570.	1.2	2
179	Evidence for a zonally trapped diurnal tide in CRISTA temperatures. Advances in Space Research, 1997, 19, 579-582.	1.2	3
180	Measurements of stratospheric trace gases by a balloon-borne infrared spectrometer in France. Journal of Atmospheric and Solar-Terrestrial Physics, 1997, 59, 1747-1755.	0.6	1

#	Article	IF	CITATIONS
181	Measurements of trace gases by the cryogenic infrared spectrometers and telescopes for the atmosphere (CRISTA) experiment. Advances in Space Research, 1997, 19, 563-566.	1.2	46
182	CFC11 measurements by CRISTA. Advances in Space Research, 1997, 19, 575-578.	1.2	9
183	Recombination energy of atomic oxygen and related species at the mesopause. Advances in Space Research, 1994, 14, 177-180.	1.2	1
184	Energy released by recombination of atomic oxygen and related species at mesopause heights. Journal of Geophysical Research, 1994, 99, 14585.	3.3	39